Earth's Future

RESEARCH ARTICLE
10.1029/2026EF008511

Climate-Driven Straightening of Western North Pacific Tropical Cyclone Trajectories

Rui Wang[1,2], Karthik Balaguru[3], Jianping Li[4], Shifei Tu[5], Quanjia Zhong[6], and Ruiqiang Ding[1,2]

[1]State Key Laboratory of Earth Surface Processes and Disaster Risk Reduction (ESPDRR), Beijing Normal University, Beijing, China, [2]Key Laboratory of Environmental Change and Natural Disasters of Chinese Ministry of Education, Beijing Normal University, Beijing, China, [3]Pacific Northwest National Laboratory (PNNL), Richland, WA, USA, [4]Frontiers Science Center for Deep Ocean Multispheres and Earth System (FDOMES)/Key Laboratory of Physical Oceanography/ Institute for Advanced Ocean Studies, Ocean University of China, Qingdao, China, [5]South China Sea Institute of Marine Meteorology, College of Ocean and Meteorology, Guangdong Ocean University, Zhanjiang, China, [6]Department of Ocean Science, Center for Ocean Research in Hong Kong and Macau (CORE), Hong Kong University of Science and Technology, Hong Kong, China

Abstract Tropical cyclone (TC) trajectory shifts remain a critical uncertainty in climate risk assessment. However, due to the absence of effective quantification methods for TC trajectories, our understanding of the overall characteristics of their trajectory shifts and the underlying impact mechanisms remains quite limited. Here, we introduce an important metric, sinuosity, as the parameter to describe the overall trajectory of TCs, and propose a new sinuosity-based machine learning framework for their classification. The findings reveal a significant decrease in the sinuosity of TC trajectories over the Western North Pacific. This reduction is mainly due to straighter trajectories within the recurving cluster TCs, which follow conventional southeast-to-northeast recurving trajectories, with most dissipating in Northeast Asia. This "straightening" phenomenon of recurving TCs is jointly driven by the shortening of TC duration and the westward expansion of the Western Pacific Subtropical High (WPSH). As the trajectories of recurving TCs are becoming straighter, they are more likely to make landfall in Northeast Asia, significantly increasing the regional risks of TCs. These findings unravel a previously unobserved dimension of TC climate response, demonstrating how changes in subtropical circulations are reshaping regional hazard patterns with profound implications for disaster preparedness, mitigation, and adaptation strategies.

Plain Language Summary Tropical cyclones (TCs) are among the most destructive natural hazards in the Western North Pacific. While changes in TC intensity and frequency have been widely studied, shifts in their trajectories remain poorly understood, partly because of the lack of a simple way to describe overall track patterns. Here, we use sinuosity to measure how curved or straight TC trajectories are, and combine it with a machine learning approach to classify trajectory types. We find that TC trajectories have become significantly straighter in recent decades. This trend is mainly driven by recurving TCs, which typically move from southeast to northeast and often affect Northeast Asia. The straightening of these trajectories is linked to shorter TC duration and the westward expansion of the Western Pacific Subtropical High. As recurving TCs become straighter, they are more likely to make landfall in Northeast Asia, potentially increasing regional disaster risk under a changing climate.

Key Points:

- A sinuosity metric quantifies tropical cyclone (TC) trajectory curvature
- TC trajectories over the Western North Pacific have become significantly straighter
- Straighter recurving trajectories increase landfall risk in Northeast Asia

Supporting Information:

Supporting Information may be found in the online version of this article.

Correspondence to:

R. Ding and Q. Zhong,
drq@bnu.edu.cn;
zqj@lasg.iap.ac.cn

Citation:

Wang, R., Balaguru, K., Li, J., Tu, S., Zhong, Q., & Ding, R. (2026). Climate-driven straightening of Western North Pacific tropical cyclone trajectories. *Earth's Future*, *14*, e2026EF008511. https://doi.org/10.1029/2026EF008511

Received 12 MAR 2026
Accepted 10 OCT 2026

Author Contributions:

Conceptualization: Rui Wang, Quanjia Zhong, Ruiqiang Ding
Data curation: Rui Wang
Formal analysis: Rui Wang
Funding acquisition: Karthik Balaguru, Quanjia Zhong, Ruiqiang Ding
Investigation: Rui Wang
Methodology: Rui Wang, Quanjia Zhong, Ruiqiang Ding
Software: Rui Wang
Visualization: Rui Wang
Writing – original draft: Rui Wang
Writing – review & editing: Rui Wang, Karthik Balaguru, Jianping Li, Shifei Tu, Quanjia Zhong, Ruiqiang Ding

© 2026 The Author(s). Earth's Future published by Wiley Periodicals LLC on behalf of American Geophysical Union. This is an open access article under the terms of the Creative Commons Attribution License, which permits use, distribution and reproduction in any medium, provided the original work is properly cited.

1. Introduction

Tropical cyclones (TCs) are powerful and destructive weather systems that can cause significant damage to ecosystems and human activities in the coastal regions (Emanuel, 2003; Feng et al., 2022; Qin et al., 2024; Shan et al., 2023). The Western North Pacific (WNP) is the most active basin globally in terms of TC activity, accounting for approximately 33% of global TC frequency (Li & Zhou, 2024). Changes in TC trajectories can shift the spatial extent and location of affected regions, making it essential to identify these changes for effective disaster prevention and mitigation.

Previous studies have predominantly focused on the long-term changes in specific characteristics of TCs, such as the locations of genesis, landfall, and lifetime-maximum intensity (LMI) (Cao et al., 2020; T. Chen et al., 2022; Jian et al., 2024; Kossin et al., 2014). These studies have reported significant poleward and coastward migrations

occurring globally in a warming world, especially in the WNP (Cao et al., 2020; T. Chen et al., 2022; Jian et al., 2024; Kossin et al., 2014; S. Wang & Toumi, 2021). Such tendencies can cause shifts in the affected latitudinal regions, alterations in TC-related regional water resources, and even a shortening of TC durations (Peduzzi et al., 2012; Pielke et al., 2003; Tu et al., 2024; Q. Zhang et al., 2009). However, knowledge gaps still exist regarding changes in WNP TC trajectory geometry over recent decades and their potential regional impacts. In general, changes in TC trajectories modify the spatial distribution of precipitation, which in turn influences the occurrence and severity of related disasters, in extreme cases leading to the displacement of millions of people (Desai et al., 2021; Kam et al., 2024; Kossin, 2018). Therefore, research in this area is of great significance. Previous work found no significant long-term trend in WNP TC sinuosity during 1951–2008 (Terry & Feng, 2010), leaving changes in recent decades and spatial differences among trajectory types unclear. Sinuosity alone also does not describe the spatial characteristics of TC trajectories, motivating its combination with spatial trajectory features for trajectory classification.

In this paper, we use an important metric, sinuosity (Terry & Feng, 2010), as the parameter to describe the overall trajectory of TCs (see Methods), and then propose a new sinuosity-based machine learning framework for classifying them. We examine changes in WNP TC trajectory sinuosity across different trajectory types during 1982–2023, as well as the associated environmental conditions and regional implications for Northeast Asia. CMIP6 HighResMIP simulations are further used to assess the representation of the observed basin-wide changes in WNP TC trajectory sinuosity in climate models.

2. Methods

2.1. Best Track Data and Reanalysis Data

In this study, TC best-track data are obtained from the International Best Track Archive for Climate Stewardship (IBTrACS, Version v04r01) during 1982–2023, which include the center locations, maximum sustained wind speeds, and landfall information of TCs (Knapp et al., 2010). We only consider TCs that occur over the WNP from July to October, with a maximum sustained wind above 34 knots (kt; 1 kt = 0.51 m s^{-1}) (Luo et al., 2022). TCs are included if their trajectories enter the defined WNP domain, regardless of where they form.

The environmental variable fields are obtained from the fifth-generation European Centre for Medium-Range Weather Forecasts (ECMWF) atmospheric reanalysis (ERA5) dataset (Hersbach et al., 2020), which include geopotential height, convective available potential energy (CAPE), and horizontal wind fields.

An additional dataset, the globally homogenized satellite-based TC record ADT-HURSAT (Kossin et al., 2020), is also used to verify the observed trend in TC trajectory sinuosity.

2.2. Environmental Background Fields

The vertical wind shear (VWS) is defined as the difference in winds between 200 and 850 hPa (Velden & Sears, 2014):

$$\mathrm{VWS} = \sqrt{(U_{200} - U_{850})^2 + (V_{200} - V_{850})^2}, \tag{1}$$

where U_{200} (V_{200}) and U_{850} (V_{850}) indicate the zonal (meridional) winds at 200 and 850 hPa, respectively.

The potential intensity (PI) represents the theoretical upper bound of TC maximum wind speed under given thermodynamic conditions (Bister & Emanuel, 2002):

$$V_{\mathrm{PI}} = \sqrt{\frac{C_k}{C_D}\frac{T_s - T_o}{T_o}\left(k_s^* - k\right)}, \tag{2}$$

where C_k and C_D are the exchange coefficients for enthalpy and momentum, T_s is the sea surface temperature, T_o is the outflow temperature, k_s^* is the saturated enthalpy at the sea surface, and k is the near-surface air enthalpy.

The steering flow is defined as the deep-layer mean wind that governs the large-scale advection of TCs. It is calculated as the pressure-weighted mean wind between 850 and 200 hPa (Luo et al., 2022):

$$\vec{V}_{\mathrm{SF}} = \frac{\int_{200}^{850} \vec{V}(p)\, dp}{\int_{200}^{850} dp}, \tag{3}$$

where $\vec{V}(p)$ denotes the horizontal wind vector at pressure level p.

We use the Western Ridge Point Index (WRPI) to quantify both the positional shifts and intensity changes of the Western Pacific Subtropical High (WPSH) (Kossin et al., 2020; Terry & Feng, 2010), which is defined as the longitude of the westernmost 5,880 gpm contour in the 500 hPa geopotential height field over the region 10°–60°N and 90°–180°E (Liu et al., 2012).

For the environmental field analysis, the environmental variables are extracted during the lifetime of each TC according to its activity time and then composited.

2.3. Definition of Sinuosity

As an important parameter in fluvial morphology, the sinuosity was originally used to describe the curvature of rivers (Terry & Feng, 2010; Terry & Gienko, 2019). In this paper, the sinuosity of the TC trajectory is defined as the ratio of total distance (TD) traveled by a TC during its lifetime to the straight-line distance (SLD) between its genesis and dissipation locations (Figure S1 in Supporting Information S1). The distances between two TC positions are calculated along the great-circle distance, which represents the shortest spherical arc length between two points on the Earth's surface. The time series of sinuosity are constructed from the mean values of all TCs in the WNP basin and in the respective clusters.

2.4. Sinuosity-Based Machine Learning Clustering Framework

To classify TCs with distinct trajectory characteristics, we develop a sinuosity-based trajectory classification framework implemented using agglomerative hierarchical clustering, an unsupervised machine learning technique. The clustering aims to identify overall spatial trajectory patterns rather than trajectory shape alone. Therefore, it is primarily based on the TC sinuosity, supplemented by genesis location, dissipation location, and the westernmost location of TCs to enhance the characterization of trajectory features. All features are standardized using z-score normalization (Al-Faiz et al., 2019; Z. Zhang et al., 2014). We then compute the pairwise Euclidean distance matrix and perform agglomerative hierarchical clustering using Ward's linkage method, which minimizes the total within-cluster variance at each merging step (Everitt et al., 2011; Murtagh & Legendre, 2014). The number of clusters is set to three based on visual inspection of the dendrogram and the interpretability of the resulting clusters. A sensitivity analysis using four to six clusters shows that the recurving trajectory type represented by Cluster 3 remains identifiable (Figure S2 in Supporting Information S1). The clustering results are visualized using a scatter plot of TC sinuosity colored by cluster membership, and further analysis is conducted for each cluster (Figure S3 in Supporting Information S1). It should be pointed out that the clustering model we developed is deterministic, eliminating random initialization processes, and thus consistently produces interpretable results. It employs a small set of physically meaningful and easily computed TC features, enabling efficient and robust classification of TC trajectories.

The Northeast Asia domain is defined as 30°–45°N and 125°–155°E, encompassing Northeast China, the Korean Peninsula, and Japan, which are the main dissipation and landfall regions of Cluster 3 TCs. Landfalling Cluster 3 TCs refer to those whose dissipation locations are within this domain and that make landfall at least once during their lifetimes. Each landfalling TC is counted only once, regardless of the number of landfalls during its lifetime.

2.5. Statistical Analysis

The Sequential Mann-Kendall test is used to detect abrupt changes in sinuosity of TCs in the entire WNP basin (C. Fu & Wang, 1992; Helsel & Hirsch, 2002), thereby enabling the partitioning of the study period into two distinct phases. Based on this test, significant abrupt changes are observed around 1983, 1986, and 1999 (Figure 1b). We select 1999 as the dividing point for the study period and split the time series into two phases because it represents the most sustained shift in sinuosity and provides sufficiently long sample sizes for both periods, whereas earlier candidates would result in very short segments and statistically less stable estimates.

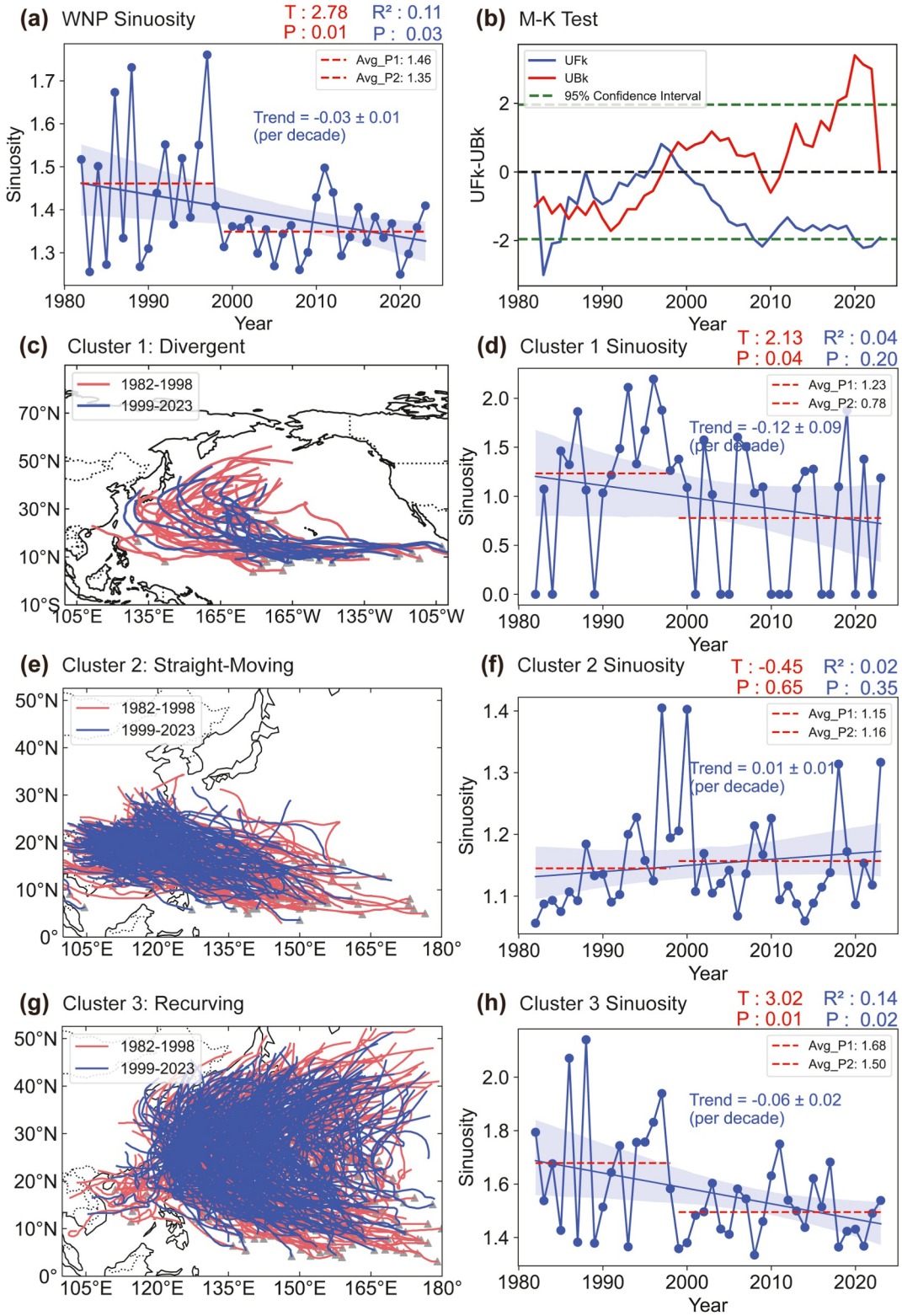
(a) WNP Sinuosity
T : 2.78 R² : 0.11
P : 0.01 P : 0.03
Avg_P1: 1.46
Avg_P2: 1.35
Trend = -0.03 ± 0.01
(per decade)
Sinuosity
Year
(b) M-K Test
UFk
UBk
95% Confidence Interval
UFk-UBk
Year
(c) Cluster 1: Divergent
1982-1998
1999-2023
(d) Cluster 1 Sinuosity
T : 2.13 R² : 0.04
P : 0.04 P : 0.20
Avg_P1: 1.23
Avg_P2: 0.78
Trend = -0.12 ± 0.09
(per decade)
Sinuosity
Year
(e) Cluster 2: Straight-Moving
1982-1998
1999-2023
(f) Cluster 2 Sinuosity
T : -0.45 R² : 0.02
P : 0.65 P : 0.35
Avg_P1: 1.15
Avg_P2: 1.16
Trend = 0.01 ± 0.01
(per decade)
Sinuosity
Year
(g) Cluster 3: Recurving
1982-1998
1999-2023
(h) Cluster 3 Sinuosity
T : 3.02 R² : 0.14
P : 0.01 P : 0.02
Avg_P1: 1.68
Avg_P2: 1.50
Trend = -0.06 ± 0.02
(per decade)
Sinuosity
Year

Figure 1.

The Student's *t*-test is applied to assess differences between two groups. The Pearson correlation coefficient (Moore et al., 2021) is used to calculate correlations between various variables. All trends in this study are determined through linear regression, and the Durbin-Watson test is applied to verify the absence of autocorrelation in the residuals. To examine changes in TC intensity, we classify TCs based on their LMI using the Saffir-Simpson Hurricane Wind Scale (Camelo & Mayo, 2021), which provides a clearer understanding of storm strength variations over time.

2.6. CMIP6 Model Analysis

High-resolution climate model outputs from the CMIP6 HighResMIP experiments (Eyring et al., 2016; Haarsma et al., 2016) are analyzed to examine how climate model simulations represent the observed change in TC trajectory sinuosity across the WNP basin. We use tropical storm track data from the CMIP6 HighResMIP Tropical Storm Tracks dataset (Roberts, 2019), which provides objectively tracked storms from a subset of HighResMIP high-resolution models using the TRACK algorithm (Hodges, 1994, 1999). Five highresSST-present models are available—CMCC-CM2-VHR4, CNRM-CM6-1-HR, EC-Earth3P-HR, ECMWF-IFS-HR, and MPI-ESM1-2-XR. Given that MPI-ESM1-2-XR shows intermittent years with zero TC occurrence over the WNP, suggesting unreliable tracking performance, it is excluded. The remaining four models are used to evaluate whether HighResMIP simulations can reproduce the observed decrease in the sinuosity of TC trajectories.

3. Results

3.1. Decreases in Sinuosity of TC Trajectories Over the WNP

We will begin by analyzing the time series changes in sinuosity of TC trajectories over the entire WNP basin. A statistically significant decreasing trend is observed in the time series of sinuosity, with a slope of −0.03 per decade from 1982 to 2023 (Figure 1a). This decreasing trend is further supported by an independent analysis using the ADT-HURSAT dataset (Kossin et al., 2020) (Figure S4 in Supporting Information S1). Based on the Sequential Mann-Kendall test, we select 1999 as the dividing point and split the time series into two parts (Figure 1b). The sinuosity is 1.46 during 1982–1998 (Period I) and decreases to 1.35 during 1999–2023 (Period II), with a significant difference between two periods. The peak of sinuosity is 1.76 in 1997 and drops to its lowest value of 1.25 in 2020. These results suggest that TC trajectories over the WNP have transitioned from being more curved to relatively straighter.

The trajectories of TCs over the WNP are diverse, leading to varying impacts across different regions (Camargo et al., 2007b; Chia & Ropelewski, 2002; B. Wang & Chan, 2002). To explain the observed decrease in the sinuosity of TC trajectories over the WNP, it is necessary to classify TCs to determine which types contribute to the decrease in sinuosity. Previous methods for classifying TCs are often limited to subjective analysis or clustering of parameters from quadratic function fitting (Camargo et al., 2007a, 2007b; Gaffney et al., 2007). These approaches represent trajectory shape implicitly through statistical model parameters, rather than providing a direct and physically interpretable measure of trajectory morphology. Consequently, we develop a sinuosity-based trajectory classification framework, implemented using an unsupervised machine learning clustering approach. Compared to traditional TC classification methods, this framework relies on a small set of easily computable parameters, ensuring objective and reproducible characterization of TC trajectory patterns.

Based on this machine learning classification framework, we categorize TCs over the WNP into three types (Figures 1c, 1e, and 1g; see Methods for detailed clustering process). Divergent cluster TCs (Cluster 1) exhibit dispersed and irregular trajectories, most of which dissipate over the WNP and rarely make landfall (Figure 1c).

Figure 1. Changes in sinuosity of tropical cyclone (TC) trajectories and their spatial characteristics. (a) The time series of sinuosity of TC trajectories over the entire western North Pacific (WNP) basin during 1982–2023. (b) Sequential Mann-Kendall test for sinuosity of TCs over the WNP during 1982–2023. Green dashed lines represent the 95% confidence level, and the intersection of red and blue solid lines represents the point of abrupt change. (c, e, and g) Spatial characteristics of trajectories of divergent cluster TCs (Cluster 1), straight-moving cluster TCs (Cluster 2), and recurving cluster TCs (Cluster 3), respectively. Based on the Sequential Mann-Kendall abrupt change point, the study period can be divided into 1982–1998 (Period I, red curves), and 1999–2023 (Period II, blue curves). Gray triangles indicate TC genesis locations. (d, f, h) The time series of sinuosity for different types of TCs. In (a, d, f, h), blue solid lines show linear regression, and red dashed lines indicate average values for Period I and II. Statistical significance of linear regression and Student's *t*-test results are shown in the top-right corner with corresponding colors.

The trajectories of straight-moving cluster TCs (Cluster 2) tend to follow a near-linear trajectory, primarily dissipating in Southeast Asia, including the southeastern coast of China and Philippines (Figure 1e). Recurving cluster TCs (Cluster 3) follow conventional southeast-to-northeast recurving trajectories, with most dissipating in Northeast Asia, including Northeast China, South Korea, North Korea, and Japan (Figure 1g). Although Cluster 1 TCs and Cluster 3 TCs both contain curved trajectories, they differ substantially in their spatial patterns. Cluster 1 TC trajectories are more spatially dispersed and generally dissipate over the open WNP, whereas Cluster 3 TC trajectories typically recurve northeastward and are more closely associated with TC activity affecting Northeast Asia. Among these three types of TCs, Cluster 3 TCs occur most frequently, accounting for 53.8% of the total, and they also exhibit the greatest sinuosity (Figure S5 in Supporting Information S1). It should be noted that local TCs originating in the South China Sea (Garner et al., 2024; S. Guan et al., 2024), due to their high sinuosity caused by irregular trajectories, are also classified into Cluster 3. However, given their relatively low frequency of occurrence (2.3%, Figure S5b in Supporting Information S1), their contribution to this cluster is limited.

We then examined the changes in sinuosity of these three types of TCs, respectively (Figures 1d, 1f, and 1h). A significant decrease in sinuosity is observed in Cluster 3 TCs, with a trend of −0.06 per decade. The average difference between two periods is 0.18 (1.68 in Period I and 1.50 in Period II). In contrast, neither Cluster 1 nor Cluster 2 TCs show a significant decreasing trend in sinuosity; instead, the sinuosity of Cluster 2 TCs exhibits a weak increasing trend. Although Cluster 2 TCs generally exhibit lower sinuosity, their relative proportion does not differ significantly between Period I and Period II (Figure S5c in Supporting Information S1). Therefore, the overall decrease in WNP TC trajectory sinuosity is unlikely to be explained by an increased proportion of Cluster 2 TCs. Taken together, these results indicate that Cluster 3 TCs are the primary contributor to the basin-wide decline in TC trajectory sinuosity. Consistently, Cluster 3 TCs are the dominant trajectory type affecting Northeast Asia (Figure 1g). Beyond direct landfalls, changes in Cluster 3 trajectories also influence the broader spatial exposure of TC impacts.

3.2. Environmental Influences on Cluster 3 TC Trajectories

We next investigate the mechanisms behind the decreases in the sinuosity of Cluster 3 TC trajectories. The percentage of Cluster 3 TCs relative to the total TCs exhibits a slight upward trend (Figure S5c in Supporting Information S1). Given that Cluster 3 TCs exhibit the highest trajectory sinuosity among the three types of TCs, the decrease in their sinuosity cannot be attributed to changes in their relative percentage representation. Since the sinuosity is the ratio of the TD traveled by a TC during its lifetime to the SLD between its genesis and dissipation locations (see Methods), variations in either metric (TD or SLD) will directly affect the sinuosity of TCs. We notice a significant decrease in TD, while SLD, despite showing a decrease, does not do so significantly (Figures S6a and S6b in Supporting Information S1). This finding suggests that the reduction in sinuosity of Cluster 3 TC trajectories over the WNP is mainly attributed to the decrease in TD traveled by these TCs. Furthermore, given that the TD is determined by the duration and translation speed of TCs, a shorter duration or slower speed can lead to a decrease in their TD. Cluster 3 TCs show a significant decrease in the duration, while their translation speed rises slightly (Figures S6c and S6d in Supporting Information S1). This implies that the reduction in TD for Cluster 3 TCs primarily stems from the decrease in their duration, which is supported by a significant positive correlation between the duration and sinuosity of Cluster 3 TCs (correlation coefficient = 0.39, $p < 0.01$; Figure 2a).

There may be deeper underlying environmental causes behind the phenomenon of shortened duration of Cluster 3 TCs (Emanuel, 2005; Tu et al., 2024). In the genesis area of Cluster 3 TCs (yellow box in Figures 2e and 2f), intensified VWS and decreased CAPE suppress the early intensification and persistence of TCs, thereby preventing them from fully realizing the thermodynamic potential implied by the increased potential intensity (PI; Figure 2g). Although VWS weakens and CAPE increases as TCs move poleward (green box in Figures 2e and 2f), these changes occur only after early TC development has already been suppressed, limiting the potential of the weakened vortices to re-intensify. In addition, the shortened duration is also associated with the poleward migration of TC genesis locations (Cao et al., 2020, 2024; T. Chen et al., 2022) (see also Figure 2b). The annual mean genesis latitude is significantly negatively correlated with the annual mean TC duration (correlation coefficient = −0.737, $p < 0.001$), and this relationship remains significant after linear detrending (correlation coefficient = −0.703, $p < 0.001$). These results suggest that both the poleward shift in TC genesis and the less favorable environmental conditions in Period II may contribute to the shorter duration. Similar links between

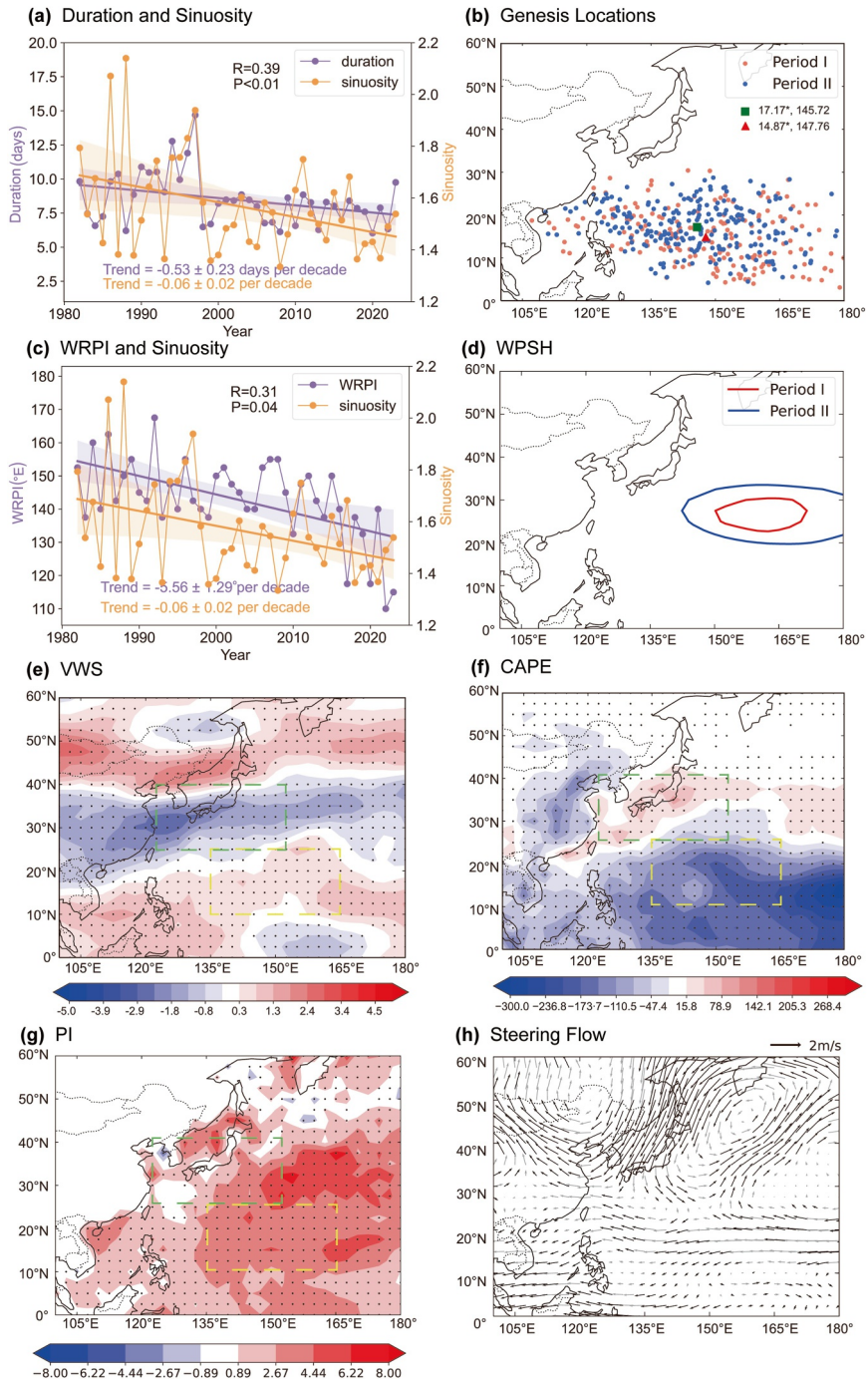

Figure 2. Environmental factors and genesis characteristics of Cluster 3 tropical cyclones (TCs). (a) The time series of the duration and the sinuosity of Cluster 3 TCs. The Pearson correlation coefficient between the two time series is shown at the top-right corner. (b) Genesis locations of Cluster 3 TCs. Red and blue points indicate TC genesis locations for 1982–1998 (Period I) and 1999–2023 (Period II), respectively. Red triangle and green square represent the mean locations in each period. The asterisk ("*") indicates significance at the 95% confidence level. (c) The time series of the Western Ridge Point Index (WRPI) and the sinuosity of Cluster 3 TCs. The Pearson correlation coefficient between the two time series is shown at the top-right corner. In (a, c), the orange lines represent the time series of sinuosity, and the purple lines represent the time series of duration or WRPI. (d) Mean locations of the Western Pacific Subtropical High (WPSH) in two periods. Red and blue lines represent the mean locations of the WPSH for Period I and Period II, respectively. (e–h) Comparison of environmental conditions during two subperiods. The differences are calculated as Period II minus Period I. (e) Vertical wind shear (VWS). (f) Convective available potential energy (CAPE). (g) Potential intensity (PI). (h) Steering flow. Dotted areas denote significant differences at the 95% confidence level. Black contours indicate regions where the differences are significant at the 95% confidence level. The yellow box highlights the TC genesis region, and the green box highlights the primary activity region of Cluster 3 TCs.

changes in TC locations and shortened duration have also been reported in the South Indian Ocean (Tu et al., 2024).

Another environmental factor associated with the sinuosity of Cluster 3 TC trajectories is the WPSH, a large-scale atmospheric system over the WNP. By modulating the genesis and dissipation locations of TCs, the WPSH plays a critical role in shaping their trajectories. Recent studies have indicated an intensification and westward extension of the WPSH, which are accompanied by a significant decrease in the WRPI (W. Guan et al., 2018; Nie et al., 2023, 2024; Zhu et al., 2023). There is a significant positive correlation between the WRPI and sinuosity of Cluster 3 TCs (correlation coefficient = 0.31, $p < 0.05$; Figure 2c), indicating an association between the westward extension of the WPSH and changes in Cluster 3 TC trajectories. The westward extension of the WPSH modifies the large-scale steering environment experienced by recurving TCs (Figures 2d and 2h), which may influence their overall trajectory evolution. Together with the shortened TC duration described above, these changes may contribute to TC trajectories becoming straighter, leading to the observed reduction in sinuosity.

3.3. Increased TC Risks in Northeast Asia

The trajectories of Cluster 3 TCs becoming straighter would alter the spatial distribution of affected regions. We compare the occurrence frequency, dissipation locations, and intensity of Cluster 3 TCs between Period I and Period II. The TC occurrence frequency shows a decreasing trend in the region south of 20°N and east of 140°E, while an increasing trend is observed in the region north of 20°N and west of 140°E, particularly near Northeast Asia (including Japan, the Korean Peninsula, and Northeast China; Figure 3a).

In addition to occurrence frequency, the dissipation frequency of Cluster 3 TCs also experiences an increasing trend in Northeast Asia (Figure 3b). We delineate a specific area (boxed region) to analyze the changes in dissipation locations of TCs in Northeast Asia (30°–45°N, 125°–155°E; Figures 3c and 3d). Within this area, we observe a significant increase in both the total frequency of Cluster 3 TCs and the frequency of landfalling Cluster 3 TCs. During Period I, the total number of Cluster 3 TCs in the area accounts for 43.4% of all Cluster 3 TCs, with a mean annual frequency of 4.41 per year. In contrast, during Period II, this percentage increases significantly to 60.8%, with a mean annual frequency of 5.84 per year. Similarly, the percentage of landfalling Cluster 3 TCs within the area relative to all Cluster 3 TCs rises significantly from 25.4% to 39.2%, with the mean annual frequency increasing from 2.59 per year in Period I to 3.76 per year in Period II (Figure 3e and Figure S7 in Supporting Information S1). To further understand the increase in TC activity over Northeast Asia, we examined the behavior of Cluster 3 TCs after entering the region (Table S1 in Supporting Information S1). The annual mean number of Cluster 3 TCs entering Northeast Asia remains nearly unchanged between the two periods, while fewer TCs continue beyond the region and more dissipate within Northeast Asia in Period II. Meanwhile, no significant change is found in the overall straight-line trajectory direction, suggesting that the increase in regional TC activity is more closely associated with changes in the subsequent trajectory behavior than with a systematic change in trajectory direction. A comparison of all trajectory clusters indicates that the increase in TC activity over Northeast Asia is primarily associated with Cluster 3 TCs. Cluster 3 TCs account for 93.8% and 97.3% of all TCs dissipating within the region during Periods I and II, respectively, whereas Cluster 1 TCs and Cluster 2 TCs contribute much less.

The intensity of TCs plays a crucial role in determining their destructive potential (Emanuel, 2005). According to the Saffir-Simpson Hurricane Wind Scale (Camelo & Mayo, 2021), Cluster 3 TCs can be divided into two groups: tropical storm–Category 2 TCs (TS–Cat2) and Category 3–5 TCs (Cat3–Cat5), with the latter group representing higher intensity. For all Cluster 3 TCs, the percentage of Cat3–Cat5 TCs increases slightly from 38.7% in Period I to 42.9% in Period II (Figure 3f and Figure S8b in Supporting Information S1). Within the designated Northeast Asia region, both total and landfalling Cluster 3 TCs show a noticeable trend of shifting toward higher intensity categories (Figures 3g and 3h; Figures S8d and S8f in Supporting Information S1). Specifically, the frequency of Cat3–Cat5 TCs increases from 1.71 per year in Period I to 2.88 per year in Period II, and their percentage also rises from 38.7% to 49.3% (Figure 3g and Figure S8d in Supporting Information S1). Likewise, among the landfalling Cluster 3 TCs, the frequency of Cat3–Cat5 TCs increases significantly from 1.0 per year to 2.12 per year, with the percentage increasing from 38.6% to 56.4% (Figure 3h and Figure S8f in Supporting

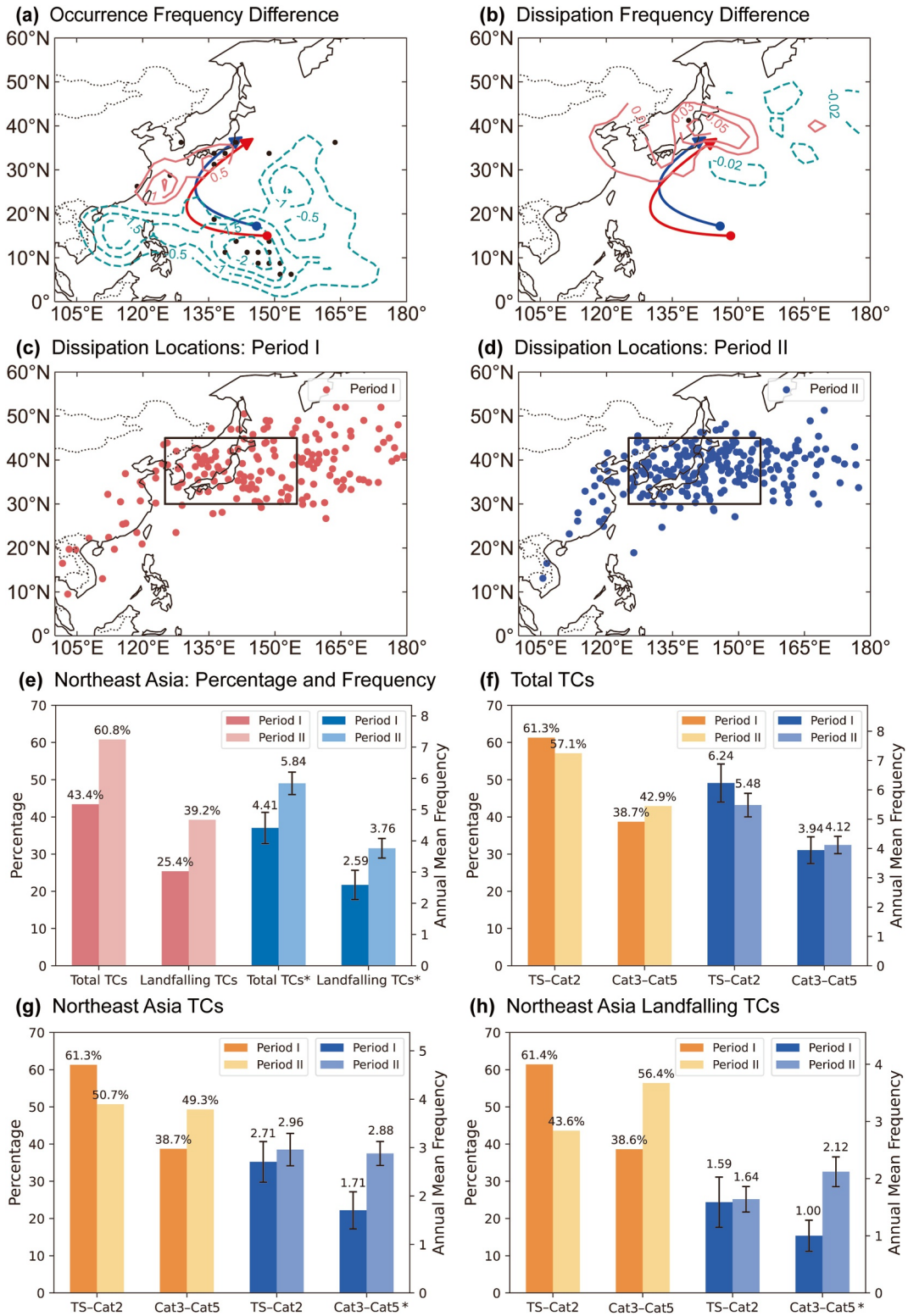
(a) Occurrence Frequency Difference
(b) Dissipation Frequency Difference
(c) Dissipation Locations: Period I
(d) Dissipation Locations: Period II
(e) Northeast Asia: Percentage and Frequency
(f) Total TCs
(g) Northeast Asia TCs
(h) Northeast Asia Landfalling TCs
Period I
Period II
Percentage
Annual Mean Frequency
Total TCs
Landfalling TCs
Total TCs*
Landfalling TCs*
TS-Cat2
Cat3-Cat5
Cat3-Cat5*

Figure 3.

Information S1). A representative case is Super Typhoon Lingling (2019). As one of the strongest TCs to affect the Korean Peninsula, Lingling caused catastrophic impacts, along with extensive agricultural damage affecting approximately 216,000 ha of cropland in Northeast China (Moon & Ha, 2021; X. Zhao et al., 2025).

The aforementioned results indicate that the straightening of Cluster 3 TC trajectories is accompanied by increases in the frequency and intensity of TC activity affecting Northeast Asia, which may lead to more severe TC-related disasters in the region. Particularly, these changes in TCs are likely to alter regional precipitation patterns, which could potentially result in a redistribution of water resources (Kossin, 2018; Rappaport, 2000). Furthermore, the impacts on offshore wind resources and the risks of TC-induced power outages should also be taken into consideration (Balaguru et al., 2023; Lipari et al., 2024; Rice et al., 2025). Additionally, the reduction in sinuosity may have implications for TC trajectory forecasting. For instance, a reduction in the number of turning points along TC trajectories can decrease the uncertainty in trajectory predictions, potentially leading to improved forecast skill (Elsberry & Carr, 2000; Krishnamurti et al., 1999; Wu & Emanuel, 1995). Future research could integrate the sinuosity to refine TC trajectory forecasting models.

4. Discussion

This study introduces an important metric, sinuosity, to quantify the overall changes in TC trajectories over the WNP. The sinuosity of TC trajectories over the WNP exhibits a statistically significant decreasing trend during 1982–2023, at a rate of −0.03 per decade. The observed decrease indicates a systematic straightening of TC trajectories over the WNP during the past four decades. Further analysis conducted with a sinuosity-based machine learning classification framework classifies TCs into three trajectory types. Cluster 1 TCs show a decreasing tendency in sinuosity, but the trend is not significant, while Cluster 2 TCs exhibit a weak increasing trend. Taken together, these results suggest that the decrease in sinuosity of TC trajectories over the WNP is primarily attributed to a reduction in sinuosity among TCs within the recurving cluster (Cluster 3). Subsequent analysis shows that the decrease in sinuosity of Cluster 3 TCs is largely driven by a shortening of their duration, which is associated with less favorable environmental conditions in Period II, including enhanced VWS and reduced CAPE in the genesis region, together with a poleward shift in genesis. Additionally, the westward extension of the WPSH modifies the large-scale steering environment and may also contribute to the observed decrease in sinuosity (see Figure 4 for the schematic diagram).

To assess whether the identified decrease in TC trajectory sinuosity depends on the sinuosity-based machine learning classification framework, we also analyzed all TCs entering a broader Northeast Asia region (north of 30°N and 120°E–155°E), regardless of cluster membership. Their mean annual sinuosity decreases significantly from 1.570 in Period I to 1.468 in Period II ($p = 0.020$), indicating that a similar decrease can also be identified without applying the classification framework. The geographical selection identifies TCs according to the region they affect, whereas the clustering approach distinguishes trajectory types using sinuosity together with spatial trajectory characteristics. Finally, we analyze four CMIP6 high-resolution models participating in HighResMIP (see Methods). The results show that three of them also exhibit a decreasing trend in TC trajectory sinuosity, indicating that a similar change is represented in most of the analyzed HighResMIP simulations (Figure S9 in Supporting Information S1).

In this study, we have only utilized the sinuosity and sinuosity-based machine learning classification framework to investigate the long-term variations in TC trajectories over the WNP. However, these methodologies can be broadly applied to explore TC trajectory changes across different ocean basins. In the context of ongoing global warming, notable alterations in TC trajectories are anticipated in multiple regions. Therefore, it is necessary to

Figure 3. Differences in occurrence frequency, dissipation locations and intensity of Cluster 3 tropical cyclones (TCs) between two periods. Differences in (a) occurrence frequency and (b) dissipation frequency of Cluster 3 TCs during 1982–1998 (Period I) and 1999–2023 (Period II). The differences are calculated as Period II minus Period I. The pink solid lines represent positive values, while the green dashed lines represent negative values. The contour intervals are 0.5 for (a) and 0.01 for (b). The thick solid lines with arrows denote the prevailing TC trajectories, with red and blue lines representing Period I and Period II, respectively. Dotted areas denote significant differences at the 95% confidence level. (c, d) Dissipation locations of Cluster 3 TCs in both periods, with the box highlighting the Northeast Asia region. (e) Percentage and frequency of total and landfalling Cluster 3 TCs in the Northeast Asia box. (f–h) Distributions of Cluster 3 TC intensity based on the Saffir-Simpson Hurricane Wind Scale. (f) Total Cluster 3 TCs; (g) Cluster 3 TCs in the Northeast Asia box; (h) Landfalling Cluster 3 TCs in the Northeast Asia box. In (e–h), the left four bars show percentage, and the right four bars show the corresponding annual mean frequency. The asterisk ("*") indicates significance at the 95% confidence level.

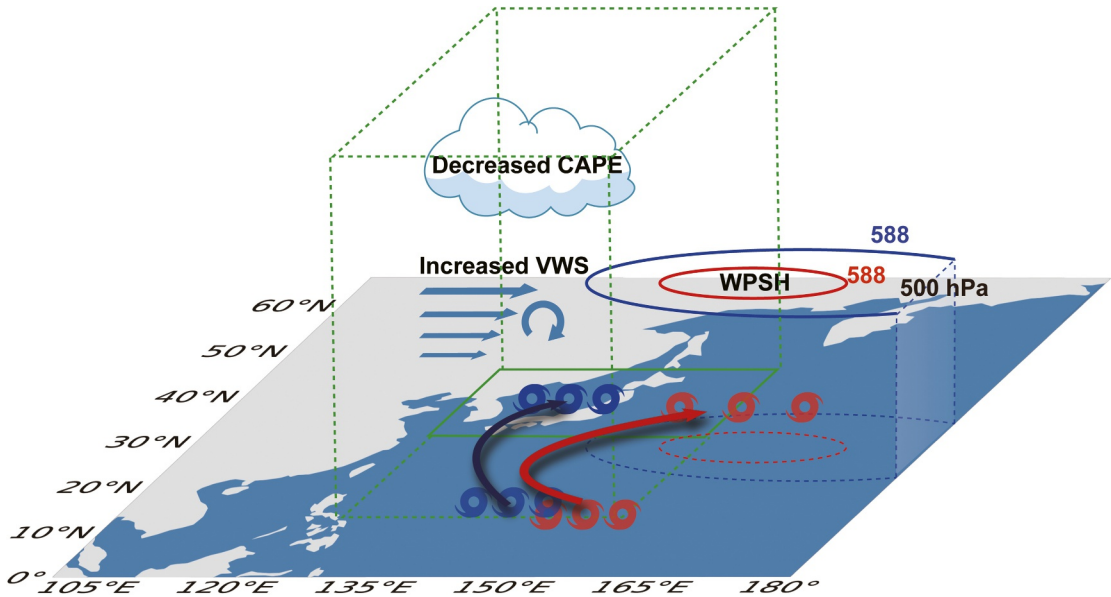

Figure 4. Schematic illustration of environmental factors driving Cluster 3 TC motions in the Western North Pacific (WNP). The red and blue TC symbols represent Cluster 3 tropical cyclones (TCs) over the WNP during 1982–1998 (Period I; red) and 1999–2023 (Period II; blue), respectively. The thick red and blue solid arrows indicate the prevailing TC trajectories during Period I (red) and Period II (blue), respectively. The red and blue ellipses denote the extent of the Western Pacific Subtropical High (WPSH) in the two periods, highlighting its westward expansion from Period I (red) to Period II (blue). The green rectangular area outlines the main region facing increased TC risks. The green dashed 3D box represents the environmental background influencing Cluster 3 TCs, including increased vertical wind shear (VWS) and reduced convective available potential energy (CAPE).

conduct further research to examine the specific characteristics of these changes and evaluate their potential impacts on regional hazard exposure and risk levels. In addition, previous work has highlighted close linkages between North Pacific TC activity and large-scale climate variability, including changes in TC track density and cluster hotspots, as well as interactions with El Niño diversity (Z.-H. Fu et al., 2025; Q. Wang et al., 2026; J. Zhao et al., 2020). In this context, future study should investigate the potential roles of these climatic factors in the observed straightening of WNP TC trajectories and assess whether this trend will persist under ongoing global warming, particularly in light of the projected westward expansion of the WPSH (X. Chen et al., 2020; Ding et al., 2024). If the observed straightening continues, the likelihood of Cluster 3 TCs making landfall in Northeast Asia may further increase, amplifying regional risks. Conducting long-term projections using high-resolution climate models will help deepen understanding of this issue, provide a scientific basis for developing adaptive strategies, and thereby mitigate escalating disaster risks over Northeast Asia.

Conflict of Interest

The authors declare no conflicts of interest relevant to this study.

Availability Statement

The data that support the findings of this study are publicly available. The TC best-track data are obtained from the International Best Track Archive for Climate Stewardship (IBTrACS v4r01), which is described by Knapp et al. (2010) and archived as the Version 4r01 data set by Gahtan et al. (2024). The environmental variables are obtained from the ERA5 reanalysis (Hersbach et al., 2020), with the hourly pressure-level and single-level data sets available from Copernicus Climate Change Service (2023a, 2023b). The Advanced Dvorak Technique–Hurricane Satellite (ADT-HURSAT) data set used in this study is described in Kossin et al. (2020) and is provided in Supporting Information S1 accompanying that article. TC tracks extracted from CMIP6

HighResMIP simulations are available from Roberts (2019). The code used in this study (v1.0.0) is archived on Zenodo (R. Wang, 2026).

Acknowledgments
This research was supported by the National Natural Science Foundation of China (Grants 42225501 and U2442208). Quanjia Zhong was supported by the Areas of Excellence Scheme of the Hong Kong Research Grants Council (Grant AoE/P-601/23-N) and the Center for Ocean Research in Hong Kong and Macau (CORE). CORE is a joint research center between Laoshan Laboratory and the Hong Kong University of Science and Technology. K.B. was supported by the U.S. Department of Energy (DOE) Office of Science Biological and Environmental Research (BER) as part of the Regional and Global Model Analysis (RGMA) program area through the Water cycle: Modeling of Circulation, Convection, and Earth system Mechanisms (WACCEM) scientific focus area and through the collaborative, multiprogram Integrated Coastal Modeling (ICoM) project. The Pacific Northwest National Laboratory is operated for U.S. DOE by Battelle Memorial Institute under contract DE-AC05-76RL01830.

References

Al-Faiz, M., Ibrahim, A., & Hadi, S. (2019). The effect of Z-Score standardization (normalization) on binary input due the speed of learning in back-propagation neural network. *Iraqi Journal of Information and Communications Technology*, *1*(3), 42–48. https://doi.org/10.31987/IJICT.1.3.41

Balaguru, K., Xu, W., Chang, C.-C., Leung, L. R., Judi, D. R., Hagos, S. M., et al. (2023). Increased U.S. coastal hurricane risk under climate change. *Science Advances*, *9*(14), eadf0259. https://doi.org/10.1126/sciadv.adf0259

Bister, M., & Emanuel, K. A. (2002). Low frequency variability of tropical cyclone potential intensity 1. Interannual to interdecadal variability. *Journal of Geophysical Research*, *107*(D24), ACL26–1–ACL26–15. https://doi.org/10.1029/2001JD000776

Camargo, S. J., Robertson, A. W., Gaffney, S. J., Smyth, P., & Ghil, M. (2007a). Cluster analysis of typhoon tracks. Part I: General properties. *Journal of Climate*, *20*(14), 3635–3653. https://doi.org/10.1175/JCLI4188.1

Camargo, S. J., Robertson, A. W., Gaffney, S. J., Smyth, P., & Ghil, M. (2007b). Cluster analysis of typhoon tracks. Part II: Large-scale circulation and ENSO. *Journal of Climate*, *20*(14), 3654–3676. https://doi.org/10.1175/JCLI4203.1

Camelo, J., & Mayo, T. (2021). The lasting impacts of the Saffir-Simpson Hurricane wind scale on storm surge risk communication: The need for multidisciplinary research in addressing a multidisciplinary challenge. *Weather and Climate Extremes*, *33*, 100335. https://doi.org/10.1016/j.wace.2021.100335

Cao, X., Liu, Y., Wu, R., Bi, M., Dai, Y., & Cai, Z. (2020). Northwestwards shift of tropical cyclone genesis position during autumn over the western North Pacific after the late 1990s. *International Journal of Climatology*, *40*(3), 1885–1899. https://doi.org/10.1002/joc.6310

Cao, X., Watanabe, M., Wu, R., Chen, W., Sun, Y., Yan, Q., et al. (2024). The projected poleward shift of tropical cyclogenesis at a global scale under climate change in MRI-AGCM3.2H. *Geophysical Research Letters*, *51*(3), e2023GL107189. https://doi.org/10.1029/2023GL107189

Chen, T., Chen, S., Zhou, M., Tu, C., Zhang, A., Chen, Y., & Li, W. (2022). Northward shift in landfall locations of tropical cyclones over the western North Pacific during the last four decades. *Advances in Atmospheric Sciences*, *39*(2), 304–319. https://doi.org/10.1007/s00376-021-1077-z

Chen, X., Zhou, T., Wu, P., Guo, Z., & Wang, M. (2020). Emergent constraints on future projections of the western North Pacific Subtropical High. *Nature Communications*, *11*(1), 2802. https://doi.org/10.1038/s41467-020-16631-9

Chia, H. H., & Ropelewski, C. F. (2002). The interannual variability in the genesis location of tropical cyclones in the Northwest Pacific. *Journal of Climate*, *15*(20), 2934–2944. https://doi.org/10.1175/1520-0442(2002)015<2934:TIVITG>2.0.CO;2

Copernicus Climate Change Service. (2023a). ERA5 hourly data on pressure levels from 1940 to present [Dataset]. *Copernicus Climate Change Service (C3S) Climate Data Store (CDS)*. https://doi.org/10.24381/cds.bd0915c6

Copernicus Climate Change Service. (2023b). ERA5 hourly data on single levels from 1940 to present [Dataset]. *Copernicus Climate Change Service (C3S) Climate Data Store (CDS)*. https://doi.org/10.24381/cds.adbb2d47

Desai, B., Bresch, D. N., Cazabat, C., Hochrainer-Stigler, S., Mechler, R., Ponserre, S., & Schewe, J. (2021). Addressing the human cost in a changing climate. *Science*, *372*(6548), 1284–1287. https://doi.org/10.1126/science.abh4283

Ding, T., Gao, H., & Li, X. (2024). Increasing risk of a "hot eastern-pluvial western" Asia. *Earth's Future*, *12*(5), e2023EF004333. https://doi.org/10.1029/2023EF004333

Elsberry, R. L., & Carr, L. E. (2000). Consensus of dynamical tropical cyclone track forecasts—Errors versus spread. *Monthly Weather Review*, *128*(12), 4131–4138. https://doi.org/10.1175/1520-0493(2000)129<4131:CODTCT>2.0.CO;2

Emanuel, K. (2003). Tropical cyclones. *Annual Review of Earth and Planetary Sciences*, *31*(2003), 75–104. https://doi.org/10.1146/annurev.earth.31.100901.141259

Emanuel, K. (2005). Increasing destructiveness of tropical cyclones over the past 30 years. *Nature*, *436*(7051), 686–688. https://doi.org/10.1038/nature03906

Everitt, B. S., Landau, S., Leese, M., & Stahl, D. (2011). *Cluster analysis* (5th ed.). John Wiley & Sons. https://doi.org/10.1002/9780470977811

Eyring, V., Bony, S., Meehl, G. A., Senior, C. A., Stevens, B., Stouffer, R. J., & Taylor, K. E. (2016). Overview of the Coupled Model Intercomparison Project Phase 6 (CMIP6) experimental design and organization. *Geosci. Model Dev.*, *9*(5), 1937–1958. https://doi.org/10.5194/gmd-9-1937-2016

Feng, K., Ouyang, M., & Lin, N. (2022). Tropical cyclone-blackout-heatwave compound hazard resilience in a changing climate. *Nature Communications*, *13*(1), 4421. https://doi.org/10.1038/s41467-022-32018-4

Fu, C., & Wang, Q. (1992). The definition and detection of the abrupt climatic change. *Chinese Journal of Atmospheric Sciences*, *16*(4), 482–493. https://doi.org/10.3878/j.issn.1006-9895.1992.04.11

Fu, Z.-H., Xi, D., Xie, S.-P., Zhou, W., Lin, N., Zhao, J., et al. (2025). Shifting hotspot of tropical cyclone clusters in a warming climate. *Nature Climate Change*, *15*(8), 850–858. https://doi.org/10.1038/s41558-025-02397-9

Gaffney, S. J., Robertson, A. W., Smyth, P., Camargo, S. J., & Ghil, M. (2007). Probabilistic clustering of extratropical cyclones using regression mixture models. *Climate Dynamics*, *29*(4), 423–440. https://doi.org/10.1007/s00382-007-0235-z

Gahtan, J., Knapp, K. R., Schreck, C. J., Diamond, H. J., Kossin, J. P., & Kruk, M. C. (2024). International best track archive for climate stewardship (IBTrACS) project, version 4r01 [Dataset]. *NOAA National Centers for Environmental Information*. https://doi.org/10.25921/82ty-9e16

Garner, A. J., Samanta, D., Weaver, M. M., & Horton, B. P. (2024). Changes to tropical cyclone trajectories in Southeast Asia under a warming climate. *npj Climate and Atmospheric Science*, *7*(1), 156. https://doi.org/10.1038/s41612-024-00707-0

Guan, S., Jin, F.-F., Tian, J., Lin, I. I., Pun, I.-F., Zhao, W., et al. (2024). Ocean internal tides suppress tropical cyclones in the South China Sea. *Nature Communications*, *15*(1), 3903. https://doi.org/10.1038/s41467-024-48003-y

Guan, W., Ren, X., Shang, W., & Hu, H. (2018). Subseasonal zonal oscillation of the Western Pacific subtropical high during early summer. *Journal of Meteorological Research*, *32*(5), 768–780. https://doi.org/10.1007/s13351-018-8061-2

Haarsma, R. J., Roberts, M. J., Vidale, P. L., Senior, C. A., Bellucci, A., Bao, Q., et al. (2016). High resolution model intercomparison project (HighResMIP v1.0) for CMIP6. *Geoscientific Model Development*, *9*(11), 4185–4208. https://doi.org/10.5194/gmd-9-4185-2016

Helsel, D. R., & Hirsch, R. M. (2002). Statistical methods in water resources. In *Techniques of water-resources investigations* (Version 1.1 ed., Vol. 4). U.S. Geological Survey. https://doi.org/10.3133/twri04A3

Hersbach, H., Bell, B., Berrisford, P., Hirahara, S., Horányi, A., Muñoz-Sabater, J., et al. (2020). The ERA5 global reanalysis. *Quarterly Journal of the Royal Meteorological Society*, *146*(730), 1999–2049. https://doi.org/10.1002/qj.3803

Hodges, K. I. (1994). A general method for tracking analysis and its application to meteorological data. *Monthly Weather Review*, *122*(11), 2573–2586. https://doi.org/10.1175/1520-0493(1994)122<2573:AGMFTA>2.0.CO;2

Hodges, K. I. (1999). Adaptive constraints for feature tracking. *Monthly Weather Review*, *127*(6), 1362–1373. https://doi.org/10.1175/1520-0493(1999)127<1362:ACFFT>2.0.CO;2

Jian, D., Zhao, H., Klotzbach, P. J., Raga, G. B., Gao, J., Cao, J., et al. (2024). Projected poleward migration of western North Pacific tropical cyclone genesis. *Geophysical Research Letters*, *51*(16), e2024GL110031. https://doi.org/10.1029/2024GL110031

Kam, P. M., Ciccone, F., Kropf, C. M., Riedel, L., Fairless, C., & Bresch, D. N. (2024). Impact-based forecasting of tropical cyclone-related human displacement to support anticipatory action. *Nature Communications*, *15*(1), 8795. https://doi.org/10.1038/s41467-024-53200-w

Knapp, K. R., Kruk, M. C., Levinson, D. H., Diamond, H. J., & Neumann, C. J. (2010). The international best track archive for climate stewardship (IBTrACS): Unifying tropical cyclone data. *Bulletin of the American Meteorological Society*, *91*(3), 363–376. https://doi.org/10.1175/2009BAMS2755.1

Kossin, J. P. (2018). A global slowdown of tropical-cyclone translation speed. *Nature*, *558*(7708), 104–107. https://doi.org/10.1038/s41586-018-0158-3

Kossin, J. P., Emanuel, K. A., & Vecchi, G. A. (2014). The poleward migration of the location of tropical cyclone maximum intensity. *Nature*, *509*(7500), 349–352. https://doi.org/10.1038/nature13278

Kossin, J. P., Knapp, K. R., Olander, T. L., & Velden, C. S. (2020). Global increase in major tropical cyclone exceedance probability over the past four decades. *Proceedings of the National Academy of Sciences*, *117*(22), 11975–11980. https://doi.org/10.1073/pnas.1920849117

Krishnamurti, T. N., Kishtawal, C. M., LaRow, T. E., Bachiochi, D. R., Zhang, Z., Williford, C. E., et al. (1999). Improved weather and seasonal climate forecasts from multimodel superensemble. *Science*, *285*(5433), 1548–1550. https://doi.org/10.1126/science.285.5433.1548

Li, Z., & Zhou, W. (2024). Poleward migration of tropical cyclones over the western North Pacific in the CMIP6-HighResMIP models constrained by observations. *npj Climate and Atmospheric Science*, *7*(1), 161. https://doi.org/10.1038/s41612-024-00704-3

Lipari, S., Balaguru, K., Rice, J., Feng, S., Xu, W., Berg, L., & Judi, D. (2024). Amplified threat of tropical cyclones to US offshore wind energy in a changing climate. *Communications Earth and Environment*, *5*(1), 755. https://doi.org/10.1038/s43247-024-01887-6

Liu, Y., Li, W., Ai, W., & Li, Q. (2012). Reconstruction and application of the monthly Western Pacific Subtropical High indices. *Journal of Applied Meteorological Science*, *23*(4), 414–423. http://qikan.camscma.cn/en/article/id/20120404

Luo, X., Yang, L., Chen, S., Liang, D., Chan, J. C. L., & Wang, D. (2022). The decadal variation of eastward-moving tropical cyclones in the South China Sea during 1980–2020. *Geophysical Research Letters*, *49*(5), e2021GL096640. https://doi.org/10.1029/2021GL096640

Moon, M., & Ha, K.-J. (2021). Abnormal activities of tropical cyclones in 2019 over the Korean Peninsula. *Geophysical Research Letters*, *48*(7), e2020GL090784. https://doi.org/10.1029/2020GL090784

Moore, D. S., McCabe, G. P., & Craig, B. A. (2021). *Introduction to the practice of statistics* (9th ed.). Macmillan Learning. Retrieved from https://www.macmillanlearning.com/college/us/product/Introduction-to-the-Practice-of-Statistics/p/1319013384

Murtagh, F., & Legendre, P. (2014). Ward's hierarchical agglomerative clustering method: Which algorithms implement ward's criterion? *Journal of Classification*, *31*(3), 274–295. https://doi.org/10.1007/s00357-014-9161-z

Nie, J., Fang, J., & Yang, X.-Q. (2023). The mechanisms of the subseasonal zonal oscillation of the Western Pacific Subtropical High in 10–25-day period and 25–50-day period. *Climate Dynamics*, *60*(11), 3485–3502. https://doi.org/10.1007/s00382-022-06523-7

Nie, J., Fang, J., Yang, X.-Q., & Huang, Q. (2024). Subseasonal relationship between the zonal oscillation of the Western Pacific Subtropical High and the South Asia High. *Climate Dynamics*, *62*(8), 7293–7308. https://doi.org/10.1007/s00382-024-07279-y

Peduzzi, P., Chatenoux, B., Dao, H., De Bono, A., Herold, C., Kossin, J., et al. (2012). Global trends in tropical cyclone risk. *Nature Climate Change*, *2*(4), 289–294. https://doi.org/10.1038/nclimate1410

Pielke, R. A., Rubiera, J., Landsea, C., Fernández, M. L., & Klein, R. (2003). Hurricane vulnerability in Latin America and the Caribbean: Normalized damage and loss potentials. *Natural Hazards Review*, *4*(3), 101–114. https://doi.org/10.1061/(ASCE)1527-6988(2003)4:3(101)

Qin, L., Zhu, L., Liu, B., Li, Z., Tian, Y., Mitchell, G., et al. (2024). Global expansion of tropical cyclone precipitation footprint. *Nature Communications*, *15*(1), 4824. https://doi.org/10.1038/s41467-024-49115-1

Rappaport, E. N. (2000). Loss of life in the United States associated with recent Atlantic tropical cyclones. *Bulletin of the American Meteorological Society*, *81*(9), 2065–2074. https://doi.org/10.1175/1520-0477(2000)081<2065:LOLITU>2.3.CO;2

Rice, J., Balaguru, K., Staid, A., Xu, W., & Judi, D. (2025). Projected increases in tropical cyclone-induced U.S. electric power outage risk. *Environmental Research Letters*, *20*(3), 034030. https://doi.org/10.1088/1748-9326/adad85

Roberts, M. (2019). *CMIP6 HighResMIP: Tropical storm tracks* [Collection]. Centre for Environmental Data Analysis. Retrieved from https://catalogue.ceda.ac.uk/uuid/e82a62d926d7448696a2b60c1925f811/

Shan, K., Lin, Y., Chu, P.-S., Yu, X., & Song, F. (2023). Seasonal advance of intense tropical cyclones in a warming climate. *Nature*, *623*(7985), 83–89. https://doi.org/10.1038/s41586-023-06544-0

Terry, J. P., & Feng, C.-C. (2010). On quantifying the sinuosity of typhoon tracks in the western North Pacific basin. *Applied Geography*, *30*(4), 678–686. https://doi.org/10.1016/j.apgeog.2010.01.007

Terry, J. P., & Gienko, G. (2019). Quantitative observations on tropical cyclone tracks in the Arabian Sea. *Theoretical and Applied Climatology*, *135*(3), 1413–1421. https://doi.org/10.1007/s00704-018-2445-1

Tu, S., Hu, Z., Liang, M., Zhou, W., Chan, J. C. L., & Xu, J. (2024). Decreasing trend in destructive potential of tropical cyclones in the South Indian Ocean since the mid-1990s. *Communications Earth and Environment*, *5*(1), 543. https://doi.org/10.1038/s43247-024-01683-2

Velden, C. S., & Sears, J. (2014). Computing deep-tropospheric vertical wind shear analyses for tropical cyclone applications: Does the methodology matter? *Weather and Forecasting*, *29*(5), 1169–1180. https://doi.org/10.1175/WAF-D-13-00147.1

Wang, B., & Chan, J. C. L. (2002). How strong ENSO events affect tropical storm activity over the western North Pacific. *Journal of Climate*, *15*(13), 1643–1658. https://doi.org/10.1175/1520-0442(2002)015<1643:HSEEAT>2.0.CO;2

Wang, Q., Tan, Z.-M., & Li, J. (2026). Effect of accumulated energy variation of pelagic tropical cyclones over the Northeast Pacific on El Niño spatial diversity. *Journal of Climate*, *39*(21), e260171–e266279. https://doi.org/10.1175/JCLI-D-26-0171.1

Wang, R. (2026). Code for climate-driven straightening of western North Pacific tropical cyclone trajectories (Version v1.0.0) [Computer software]. *Zenodo*. https://doi.org/10.5281/zenodo.21961405

Wang, S., & Toumi, R. (2021). Recent migration of tropical cyclones toward coasts. *Science*, *371*(6528), 514–517. https://doi.org/10.1126/science.abb9038

Wu, C.-C., & Emanuel, K. A. (1995). Potential vorticity diagnostics of hurricane movement. Part 1: A case study of Hurricane Bob (1991). *Monthly Weather Review*, *123*(1), 69–92. https://doi.org/10.1175/1520-0493(1995)123<0069:PVDOHM>2.0.CO;2

Zhang, Q., Wu, L., & Liu, Q. (2009). Tropical cyclone damages in China 1983–2006. *Bulletin of the American Meteorological Society*, *90*(4), 489–496. https://doi.org/10.1175/2008BAMS2631.1

Zhang, Z., Cheng, Y., & Liu, N. C. (2014). Comparison of the effect of mean-based method and *z*-score for field normalization of citations at the level of web of science subject categories. *Scientometrics*, *101*(3), 1679–1693. https://doi.org/10.1007/s11192-014-1294-7

Zhao, J., Zhan, R., Wang, Y., Xie, S.-P., & Wu, Q. (2020). Untangling impacts of global warming and Interdecadal Pacific Oscillation on long-term variability of North Pacific tropical cyclone track density. *Science Advances*, *6*(41), eaba6813. https://doi.org/10.1126/sciadv.aba6813

Zhao, X., Wang, C., Cheng, L., & Qian, Y. (2025). Characteristics of impacts of northward typhoons on agriculture in Northeast China in 2020 and estimation of total grain yield loss. *Journal of Marine Meteorology*, *45*, 69–78. https://doi.org/10.19513/j.cnki.hyqxxb.20220825001

Zhu, Z., Zhou, Y., Jiang, W., Fu, S., & Hsu, P. (2023). Influence of compound zonal displacements of the South Asia High and the Western Pacific Subtropical High on Meiyu intraseasonal variation. *Climate Dynamics*, *61*(7), 3309–3325. https://doi.org/10.1007/s00382-023-06726-6